Multimechanism Fouling Model for Micro and Ultrafiltration Membranes for Wastewater Treatment

Tomasz Janus*[1] and Bogumil Ulanicki[2]

[1]Independent Researcher
[2]Water Software Systems, De Montfort University, LE1 9BH, Leicester, United Kingdom
* *tomasz.k.janus@gmail.com*

ABSTRACT

Fouling is a term describing progressive reduction of membrane permeability during filtration of solutes and suspensions. The problem with fouling lies in its complexity and our lack of understanding of the science behind it. In wastewater treatment applications the problem is additionally magnified by polydispersity of wastewater suspensions. For these reasons fouling models in wastewater treatment applications are usually black-box or grey-box. Theoretical/classical fouling models are available but are applied predominantly to monodisperse suspensions where one fouling mechanism dominates and hence, only one classical fouling equation suffices to describe the filtration process. In wastewater applications we need to solve several equations simultaneously in order to be able to predict different stages of the filtration process. This paper presents such a model which combines three classical fouling mechanisms: blocking, constriction and cake growth. The paper shows successful calibration results but also indicates parameter identifiability issues.

Keywords: fouling, microfiltration, mechanistic model

1 INTRODUCTION

As briefly outlined above, fouling is still not well understood, especially when the medium being filtered is polydispere such as wastewater. Due to complex nature of the fouling phenomena during filtration of wastewater suspensions, fouling models applied to wastewater treatment are usually black-box or grey-box. Such models are simpler, often easier to calibrate, and faster to execute than more complex mechanistic models but their downside is lack of generality and completeness. Meanwhile, classical mechanistic fouling models, i.e. pore constriction, complete pore blocking, intermediate pore blocking, and cake formation, as defined in [1], offer more physical description of fouling mechanisms but historically had been applied only to monodisperse suspensions where one fouling mechanism dominated over the other and only this one classical fouling model was sufficient to describe the entire course of the filtration process. In case of polydisperse suspensions such as wastewater one classical fouling mechanism cannot successfully describe the entire filtration process due to simultaneous as well as sequential occurrence of several fouling processes.

The research question, which the authors try to answer in this piece of work, is how to combine these classical fouling models into one single fouling model such that membrane fouling during filtration of various polydisperse suspensions can be accurately predicted. This problem was already attempted in several earlier publications, e.g. [2, 3]. However, some of the proposed models were either presented in an analytically derived integral form which limited their application to constant trans-membrane pressure (TMP) dead-end filtration and were based on physically incorrect assumptions [2]. For example, in [2] the authors assumed that cake grows

only on the previously blocked area and introduced the concept of *'blocked flux'* which disagrees with the original concept of pore blocking which, being an open pore area loss model, assumes that the flow through the blocked part of the membrane is null and stops as soon as the pore is blocked. As a result of this, pore blocking was not actually represented and the model was reduced to pore constriction and cake filtration only. Additionally, the model of [2] was presented in an integral form which limits its application to constant flux unstirred dead-end filtration. In [3], the authors rightfully assumed zero flux through the blocked pores and additionally modelled cake consolidation through entrapment of soluble and colloidal material. What stems from it is a reduction of the available soluble and colloidal component concentrations at the membrane surface via prefiltering effects of the cake and thus lower pore constriction and blocking rates under the cake. At the same time though, their model assumes that cake grows instantly on the entire unblocked area and that not only constriction, but also pore blocking occurs below the cake. It may be argued that these two assumptions are not physically correct.

The model presented here is based on slightly different assumptions as outlined in Section 2.1. It was successfully calibrated on the data obtained from dead-end and cross-flow filtration experiments, hence proving its ability to predict fouling on different types of membranes, configurations and with complex feeds. Since it was formulated as a system of differential and algebraic equations it can be used to simulate membrane operation under time-varying flux and pressure conditions, contrary to [2] whose models were presented in an analytically derived integral form for dead-end constant TMP filtration only. The work presented here also demonstrates the difficulty in calibrating fouling models and prompts the need for more research focused on experiment design and identification of multimechamism fouling models, such as one presented in this paper.

2 MODEL FORMULATION

The model is formulated as a system of 6 ordinary differential equations (ODEs) and 3 algebraic equations (AEs). The ODEs describe, respectively, pore blocking, cake growth, pore constriction on the unblocked membrane and under the cake, growth of area under the cake, and change of average membrane resistance under the cake. The AEs describe the relationships between TMP and the two modelled flux components (see Fig. 1) and ascertain that the sum of the blocked, unblocked and 'caked' areas on the membrane is always equal to the total membrane area A. The model contains 6 unknown parameters: α_1, α_2, β_1, β_2, $f\,R'$, $R_{c,0}/R_m$ - see Sec. 2.2.

2.1 Modelling Hypotheses

Fouling is modelled here with three classical fouling mechanisms: constriction, blocking, and cake growth. Pore blocking leads to gradual reduction of open pores and an immediate and complete reduction of flux to zero through the blocked pores. Therefore 'blocked flux' as in [2] does not exist. The model divides the membrane into three areas: blocked (A_b), unblocked (A_u), and area under the cake (A_c). Cake grows only on A_c which increases in time as cake particles keep landing on the membrane surface. The growth of A_c

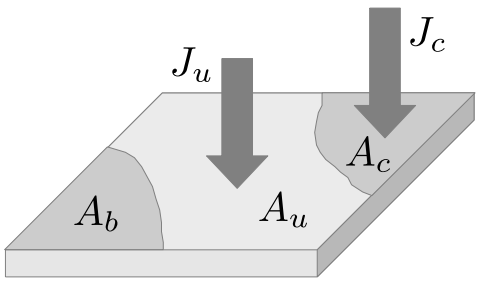

Figure 1: Graphical representation of flux split on a membrane

can be viewed as 'incomplete' pore blocking. The particles cover the membrane pores and create initial resistance $R_{c,0}$ but do not block the pores completely and hence let the flux across the membrane to continue, albeit at a diminished rate. The rate of pore constriction under the cake is slower because the flux across A_c is lower due to additional resistance created by the cake. Additionally, cake acts as a prefilter for some colloidal matter. Hence, pore constriction occurs in the pores of the unblocked membrane surface as well as under the cake. Pore blocking occurs only on the unblocked membrane with area A_u. The flux across the membrane is divided into two parts: flux through the unblocked area J_u and flux through the cake-covered area J_c.

2.2 Model Equations

2.2.1 Classical fouling equations

Pore blocking is described with complete pore blocking mechanism

$$dA_b/dt = \alpha_1 \, C_p \, J_u \, (A - A_b - A_c) \tag{1}$$

where α_1 (m^2 kg^{-1}) is the pore blocking parameter and C_p (g m^{-3}) denotes the concentration of particulate matter. Pore constriction occurs on the unblocked membrane (Eq. 2) and under the cake (Eq. 3).

$$dR_{inb}/dt = \beta_1 \left(2 \, \pi \, \phi_P \, L^3\right)^{-\frac{1}{2}} {R_{inb}}^{\frac{3}{2}} \, J_u \, C_s \tag{2}$$

$$dR_{ic}/dt = \beta_2 \left(2 \, \pi \, \phi_P \, L^3\right)^{-\frac{1}{2}} {R_{ic}}^{\frac{3}{2}} \, J_c \, C_s \tag{3}$$

in which R_{inb} and R_{ic} (m^{-1}) represent, respectively, the resistances of the unblocked membrane and membrane under cake due to pore constriction. β_1 and β_1 (m^3 kg^{-1}) are pore constriction parameters, C_s (g m^{-3}) denotes the concentration of dissolved organic matter (DOM), ϕ_P (m^{-2}) represents pore density, and L (m) is membrane thickness. ϕ_P and L are calculated from initial conditions, i.e. flow and pressure at the beginning of the filtration study. Both equations above are derived from the fundamental pore constriction equation describing a reduction of mean pore radius in time due to deposition of DOM inside the pores' inner walls. Cake growth is modelled as net increase in cake resistance R_c (m^{-1}) due to deposition of particulate matter with concentration C_p (g m^{-3}) minus the effects of cake removal due to cross-flow, see second term in Eq. 4.

$$dR_c/dt = f \, R' \, J_c \, C_p - k_r \, R_c \tag{4}$$

where k_r (s^{-1}) is the cake removal constant, R' (m kg^{-1}) is the specific cake resistance and f is a dimensionless parameter describing fraction of the particular matter contributing to cake formation. For the purpose of model identification f and R' are lumped into one calibration parameter $f \, R'$. Rate of membrane area coverage with cake is modelled with 'complete pore blocking' type equation with proportionality constant α_2. Both processes share the same type of dynamics since they both describe pore blocking with the only difference that the second one is 'incomplete', i.e. the pores are not entirely closed by the particles. In most cases the chance of a particle to completely block a pore will be lower then to block it partially, hence usually $\alpha_2 > \alpha_1$.

$$dA_c/dt = \alpha_2 \, C_p \, J_u \, (A - A_b - A_c) \tag{5}$$

2.2.2 Total resistance of membrane covered with cake

The rate of change of total resistance of cake-covered membrane $R_{c,tot}$ is given as the sum of the rate of change of resistance due to constriction under cake given in Eq. 3, rate of cake growth described with Eq. 4 and the change of membrane resistance under cake due to gradual coverage of unblocked membrane with cake layer (Eq. 5). This equation arises from the fact that in each subsequent time moment cake layer advances onto an area with different unblocked membrane resistance R_{inb} while the unblocked membrane is simultaneously undergoing pore constriction. This process is visualised in Fig. 2. Since we model the membrane as a point in space we need to calculate average resistance under the cake such that the flow through A_c with such equivalent resistance $R_{c,tot}$ is equal to the sum of flows through all individual elementary areas having different resistances.

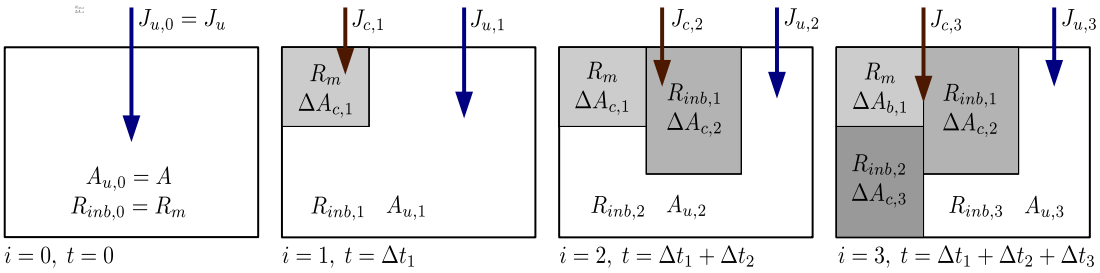

Figure 2: Cake area advancement and total resistance of cake-covered membrane $R_{c,tot}$

The equality of flow is represented with Darcy's law which relates flux to pressure and resistance.

$$\frac{\Delta P}{\mu\, R_{c,tot}(t+dt)}\,(A_c + dA_c) = \frac{\Delta P}{\mu\,\left(R_{c,tot}(t) + dR_{ic} + dR_c\right)}\,A_c + \frac{\Delta P}{\mu\, R_{inb}(t)}\,dA_c \tag{6}$$

The left side of Eq. 6 represents the flow over caked-covered area $A_c + dA_c$ at time moment $t + dt$ whilst the right side represents the sum of two flows: one across A_c with resistance $R_{c,tot}$ plus elementary increases of resistances dR_{ic} and dR_c, and the other across additional area increment dA_c with resistance $R_{inb}(t)$. After simplification and rearrangement we obtain the expression for $R_{c,tot}$ at time moment $t + dt$

$$R_{c,tot}(t+dt) = \frac{R_{inb}(t)\,\left(R_{c,tot}(t) + dR_{ic} + dR_c\right)\,(A_c + dA_c)}{A_c\,R_{inb}(t) + R_{c,tot}(t)\,dA_c + dR_{ic}(t)\,dA_c + dR_c(t)\,dA_c} \tag{7}$$

which after substitution of $R_{c,tot}(t+dt)$ with $R_{c,tot}(t) + \left.\frac{dR_{c,tot}}{dt}\right|_t dt$, i.e. the first two terms of the Taylor expansion series, and eliminating infinitesimally small terms, gives the following expression

$$\frac{dR_{c,tot}}{dt} = \frac{dR_{ic}}{dt} + \frac{dR_c}{dt} + \frac{1}{A_c}\frac{dA_c}{dt}\,R_{c,tot}\left(1 - \frac{R_{c,tot}}{R_{inb}}\right) \tag{8}$$

in which the first term is described by Eq. 3, the second term is calculated with Eq. 4 whilst the third term describes the change of resistance due to cake advancement.

2.2.3 Auxiliary algebraic equations

The ODEs are supplemented with algebraic equations (AEs) which ascertain that $A - A_u - A_b - A_c = 0$ and calculate J_u and J_c from the corresponding resistances: $R_m + R_{inb}$ and $R_m + R_{c,tot}$, given dynamic permeate viscosity μ (Pa·s) and 'clean' membrane resistance at the beginning of filtration R_m. $J_u = \frac{\Delta P}{\mu\,(R_m + R_{inb})}$, $J_c = \frac{\Delta P}{\mu\,(R_m + R_{c,tot})}$. The volumetric flows are calculated from the fluxes and the corresponding surface areas, i.e. $Q_u = J_u\,A_u$ and $Q_c = J_c\,A_c$.

2.2.4 Initial conditions

The initial conditions for Eqs. 1, 2, 3 + 8, 4, 5, and 8 are, respectively, $A_b(0) = 0$, $R_{inb}(0) = 0$, $R_{ic}(0) = 0$, $R_c(0) = R_{c,0}$, $A_c(0) = 0$, $R_{c,tot}(0) = R_{c,0}$.

3 MODEL CALIBRATION

3.1 Experimental Procedures

The model was calibrated on two sets of experimental data obtained from two different sources. For a detailed description of the experimental methods the reader is referred to the original papers of [2] and [4]. This section just outlines the most important information about the type of equipment used and the environmental conditions.

The first set of data was obtained by [2] using the 25mm dia. Amicon ultrafiltration cell model 8010 with stirring switched off and the cell operating at a constant TMP of 14kPa and a constant temperature of 20°C. Filtration was carried out on two different membranes (0.2μm polycarbonate track etched and 0.22μm hydrophobic Durapore® membrane (GVHP)), with three different solutions (polystyrene microsphere solution, bovine serum albumen (BSA) solution, and BSA solution prefiltered through 0.1μm hydrophilic Durapore® membrane). Four filtration experiments were carried out. Each experiment was performed at different solution concentration which resulted in a family of flux and resistance curves. Due to space limitation in this manuscript only three out of four experiments were used for identification.

Data for the second calibration study was obtained by [4] from a crossflow filtration cell equipped with a 0.22μm hydrophilic Millipore polyvinylidene fluoride (PVDF) membrane receiving a 100 mgL^{-1} 0.2μm sodium alginate solution at different sub-critical flux rates. For each preset flux rate the cell was operating for a period of time sufficient to observe a two-stage TMP profile, i.e. slow gradual pressure rise over a relatively long period of time followed by a rapid TMP increase. The experiment was run at 5 different subcritical flux rates of, respectively, 40, 45, 50, 55, and 60 Lm^{-2}h^{-1}. Each experiment was carried out on a virgin membrane. The critical flux for this alginate solution and membrane was determined in a separate flux stepping experiment to be 66 Lm^{-2}h^{-1}.

3.2 Numerical Methods

In the first calibration study four model parameters were calibrated in three separate calibrations: β_1, α_2, $f\,R'$, and initial resistance of cake deposit $R_{c,0}$. In this as well as the second calibration we assumed that $\alpha_1 = 0$ and $\beta_2 = 0$, i.e. no pore blocking and no constriction under cake. In the second calibration study we additionally assumed that $R_{c,0} = 0$. Thus, on both occasions we calibrated the reduced order model. The reason for this decision are parameter identifiability issues encountered during model calibration, as described later in text. The model parameters were identified in two steps: first, genetic algorithm (GA) was used to find a global minimum since the objective function looks to be non-convex; second, a Levenberg-Marquardt algorithm implemented in MATLAB function `lsqnonlin` was used to refine the solution and output the Jacobian of the objective function around the minimum necessary for the calculation of asymptotic confidence intervals of the model parameter estimates. The objective function was the sum of squared errors between measured and calculated outputs. In the first calibration experiments the errors were calculated between the predicted and measured (Q/Q_0) and R_{tot}. The data were normalised to $0 - 1$ to ascertain that the errors in flows and resistances were

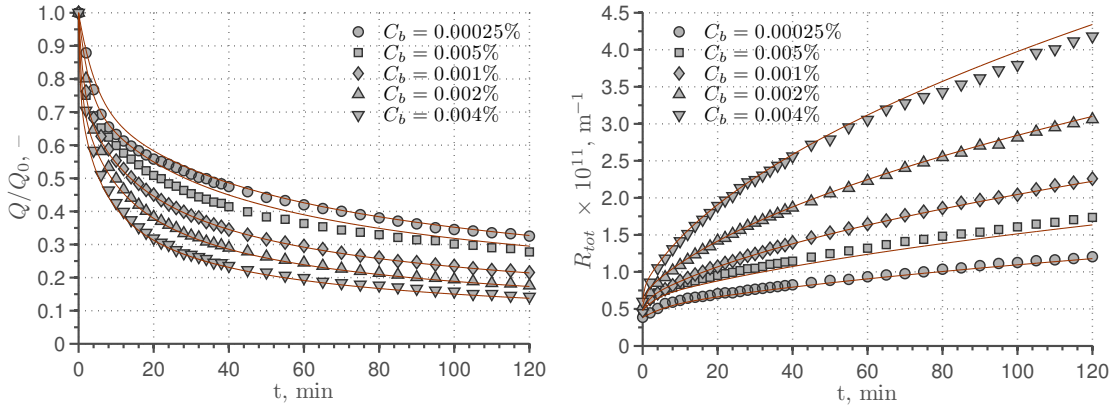

Figure 3: Flow decline and resistance increase during filtration of 0.25μm polystyrene microsphere solutions through 0.2μm polycarbonate track etched membranes.

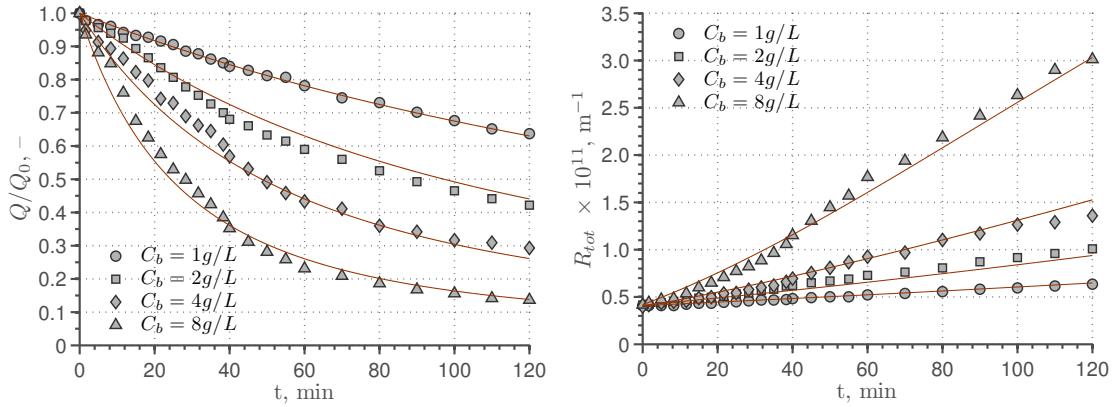

Figure 4: Flow decline and resistance increase during filtration of standard BSA solutions through 0.22μm hydrophobic Durapore membranes (GVHP).

assigned equal weights. In the second calibration study the objective function was the sum of squared errors between modelled and predicted TMP at each flux.

3.3 Constant-pressure Unstirred Dead-end Filtration

Outputs of the model are presented in Figures 3,4, and 5. The estimated parameter values together with asymptotic 95% confidence intervals are shown in Table 1 in which Exp. 1 corresponds to filtration of 0.25μm polystyrene beads through 0.2μm polycarbonate track etched membrane, Exp. 2 corresponds to filtration of standard BSA solution through 0.22μm GVHP membrane, whilst Exp 3 corresponds to filtration of 0.1μm prefiltered BSA solution through 0.22μm GVHP membrane. Clean membrane resistances R_m were calculated from initial conditions and were found to be 5.963×10^{10}, 4.184×10^{10}, and 4.622×10^{10}, respectively.

Table 1: Calibration results on dead-end constant pressure filtration data

	β_1 (m^3 kg^{-1})	α_2 (m^2 kg^{-1})	$f'R'$ (m kg^{-1})	$R_{c,0}/R_m$ (–)
1	0	$5.370 \times 10^4 \pm 6.747 \times 10^3$	$2.252 \times 10^{14} \pm 3.142 \times 10^{12}$	0.2945 ± 0.0167
2	$2.057 \times 10^{-7} \pm 1.203 \times 10^{-7}$	$2.064 \times 10^{-2} \pm 1.199 \times 10^{-1}$	$1.292 \times 10^9 \pm 5.164 \times 10^{10}$	0.5111 ± 10.22
3	$1.694 \times 10^{-7} \pm 2.708 \times 10^{-8}$	0	0	0

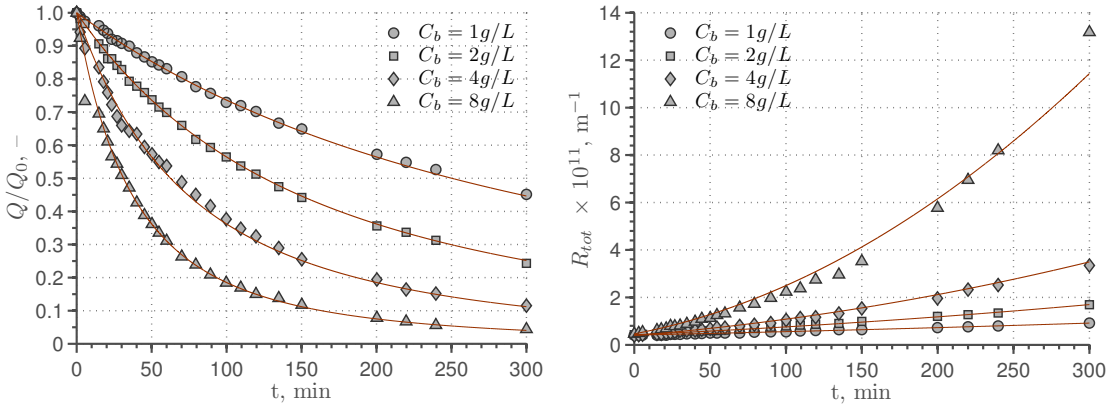

Figure 5: Flow decline and resistance increase during filtration of 0.1µm prefiltered BSA solutions through 0.22µm hydrophobic Durapore membranes (GVHP).

As demonstrated, the model fits the data reasonably well on all three occasions, however, looking at the concavity of the curves (see Fig 4), the quality of fit in Exp 2 is worse than for the other two experiments which represent the extreme cases where a single mechanism dominates fouling, i.e. cake filtration in Exp 1 and pore constriction in Exp 3 (notice zeros in Table 1). In case of Exp 2 identification proved a little more problematic resulting in worse fit and very large confidence intervals on the estimated parameters. The reason for such an outcome can be two-fold - either inappropriate model structure or inappropriate objective function. Recalibration with cake filtration replaced by pore blocking or with all processes switched on could be attempted but it has already been suspected that the information used for calibration was insufficient to attempt identification of the entire parameter set. GA was found to converge to minima with similar objective function values but different parameter estimates indicating that the objective function was non-convex. It is likely that some parameters, e.g. α_1 and $f'R'$ may also be correlated.

3.4 Constant-flux Cross-flow Filtration

Table 2: Results of model calibration on long-term constant flux filtration data of [4]

Fluxes, Lmh		60	55	50	45	40
Parameter	Unit					
$f'R' \times 10^{14}$	m kg^{-1}	3.62	1.68	0.754	1.03	0.427
α_2	m^2 kg^{-1}	454	365	88.0	43.6	10.6
$\beta_1 \times 10^2$	m^3 kg^{-1}	3.91	6.97	1.29	1.26	0.303

The curve fits resulting from the model identification based on the measured TMP curves during constant flux cross-flow filtration at 5 different subcritical fluxes are shown in Fig.6 whilst the estimated parameter values for each flux are given in Table 2. The results show good model fits with just two fouling mechanisms - pore constriction and cake formation. All estimated parameters, if plotted, show exponential dependence on flux but the amount of information provided by this single experiment is insufficient to make any of the observations conclusive.

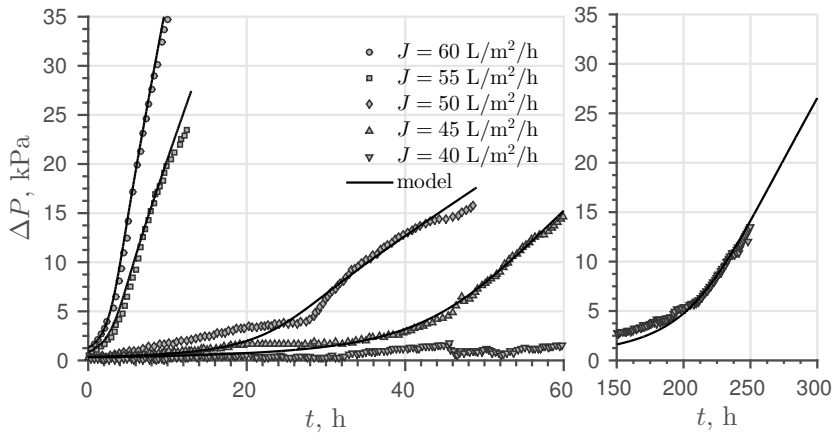

Figure 6: Calibration results on constant flux filtration data in a crossflow microfiltration cell.

4 CONCLUSIONS

Developing a single identifiable fouling model able to predict the course of filtration of different suspensions on different membranes has so far proven difficult due to complexity of the fouling phenomena, simultaneous and sequential occurrence of different fouling mechanisms, differences in hypotheses regarding the model structure, problems with identifiability on available experimental data. A candidate multimechamism fouling model was proposed in this study but the data used for identification was insufficient to calibrate and validate the full model, resulting in calibration of a reduced order model, albeit with good results. The calibration study revealed the problems with parameter identifiability which could results from improper model structure but were likely due to a poor choice of the objective function. In order to make progress in modelling membrane fouling more efforts should be concentrated on appropriate experiment design such that all measurable and observable quantities about the process are available for model identification. Additionally, more sophisticated objective functions can be formulated, e.g. exploiting the concavity of the curves by incorporating some measure of similarity between measured and simulated n exponents in the Hermia's equation [1] or partitioning the experimental data into regions where different fouling processes dominate the filtration process.

References

[1] J. Hermia, "Constant pressure blocking filtration laws - application to power-law non-newtonian fluids." *Transactions of the Institution of Chemical Engineers*, vol. 60, no. 3, pp. 183–187, 1982.

[2] C. Duclos-Orsello, W. Li, and C.-C. Ho, "A three mechanism model to describe fouling of microfiltration membranes," *Journal of Membrane Science*, vol. 280, no. 1-2, pp. 856–866, 2006.

[3] J. Wu, C. He, X. Jiang, and M. Zhang, "Modeling of the submerged membrane bioreactor fouling by the combined pore constriction, pore blockage and cake formation mechanisms," *Desalination*, vol. 279, pp. 127–134, 2011.

[4] Y. Ye, V. Chen, and A. Fane, "Modeling long-term subcritical filtration of model EPS solutions," *Desalination*, vol. 191, no. 1-3, pp. 318–327, 2006, international Congress on Membranes and Membrane Processes.